Science Advances
AAAS

advances.sciencemag.org/cgi/content/full/7/20/eabg2174/DC1

Supplementary Materials for

Insights into the molecular mechanism of amyloid filament formation: Segmental folding of α-synuclein on lipid membranes

Leif Antonschmidt, Rıza Dervişoğlu, Vrinda Sant, Kumar Tekwani Movellan, Ingo Mey, Dietmar Riedel, Claudia Steinem, Stefan Becker, Loren B. Andreas*, Christian Griesinger*

*Corresponding author. Email: land@nmr.mpibpc.mpg.de (L.B.A.); cigr@nmr.mpibpc.mpg.de (C.G.)

Published 14 May 2021, *Sci. Adv.* **7**, eabg2174 (2021)
DOI: 10.1126/sciadv.abg2174

This PDF file includes:

Figs. S1 to S11
Tables S1 to S3
References

Supplementary Materials

Supplementary Figures

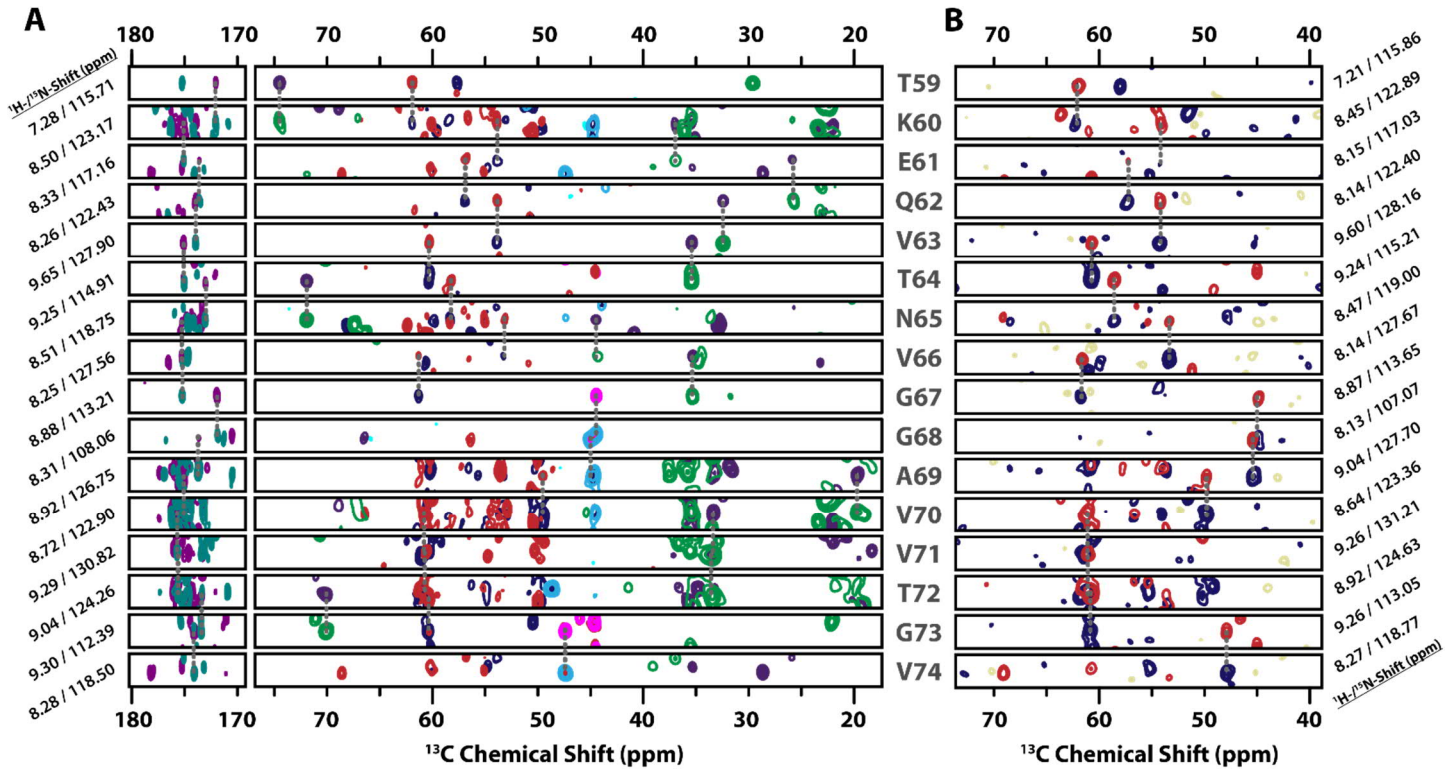

Fig. S1. Sequence assignment spectra for αS fibrils. Strip plot for a generic sequence walk along $_{59}$TKEQVTNVGGAVVTGV$_{74}$ in proton-detected 3D Spectra. (A) (H)CANH (red), (HCO)CA(CO)NH (blue), (HCA)CB(CA)NH (pink/purple); (HCA)CB(CACO)NH (light blue/dark purple), (HCA)CONH (purple), (H)CONH (teal) of ^{2}H,^{13}C,^{15}N-labelled αS fibrils spectra acquired at 800 MHz with 55 kHz MAS; (B) (H)CANH (red), (HCO)CA(CO)NH (blue) spectra of ^{13}C,^{15}N-labelled αS fibrils spectra acquired at 950 MHz with 100 kHz MAS.

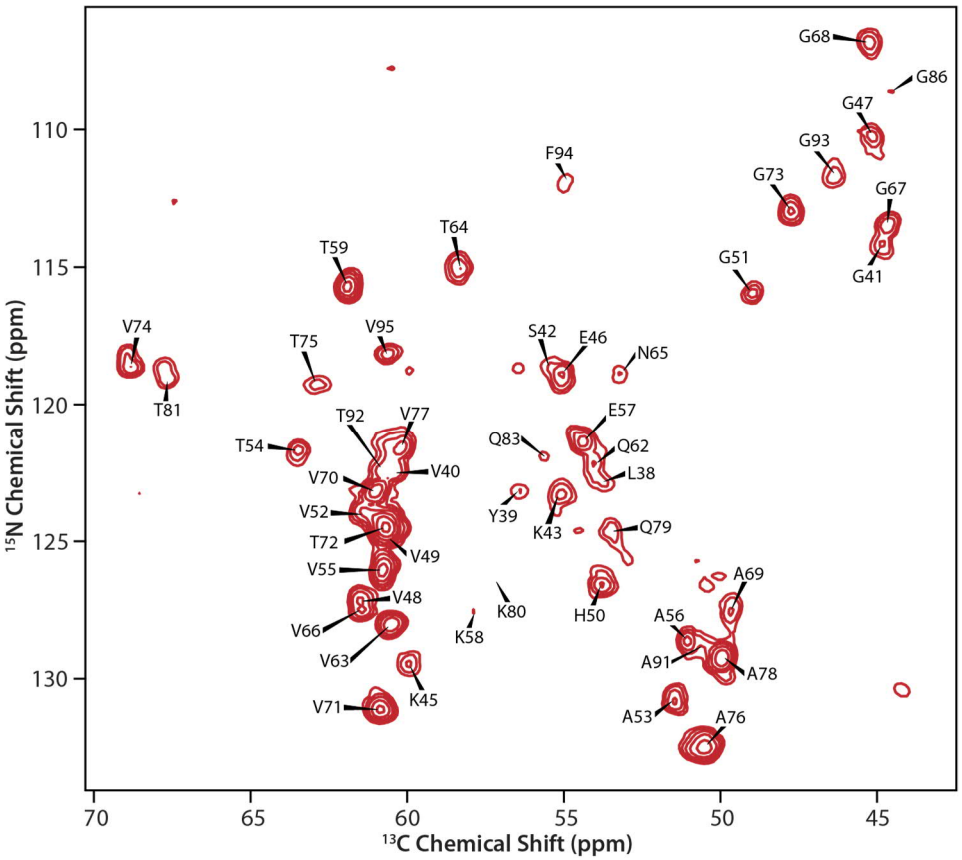

Fig. S2. Assignment of backbone resonances for αS fibrils. CN-projection of a 3D (H)CANH spectrum of ^{13}C,^{15}N-labelled αS fibrils acquired at 950 MHz with 100 kHz MAS with sequence assignments.

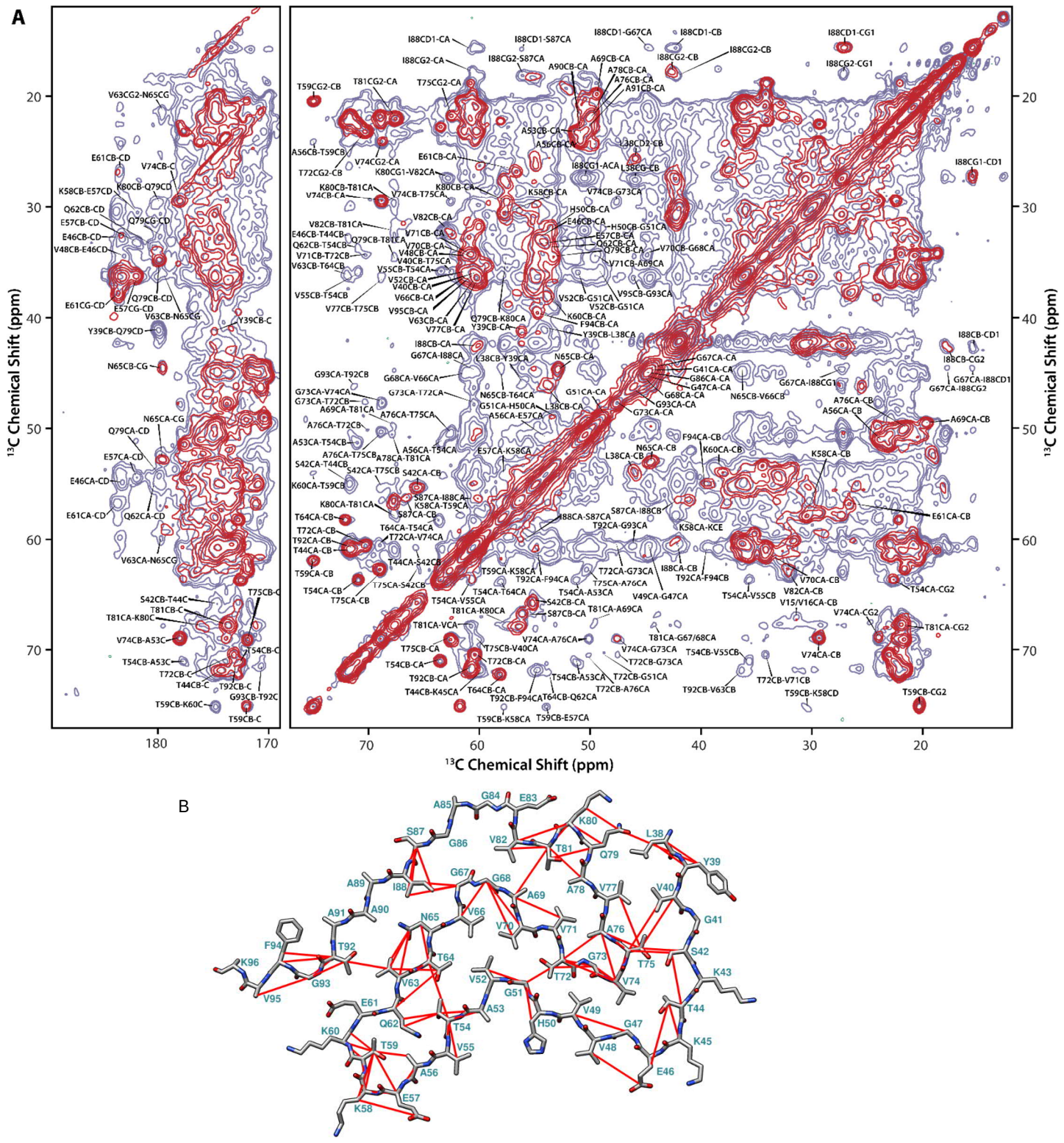

Fig. S3. Site specific contact mapping of αS. (A) ^{13}C,^{13}C correlation spectrum with DARR mixing of 200 ms of ^{13}C,^{15}N-αS fibrils acquired at 850 MHz with 17 kHz MAS with assignments; (B) Long range contacts identified from ^{13}C,^{13}C DARR spectra mapped onto the structure of Polymorph 2a (PDB 6ssx). Fibrils were prepared in the presence of POPA/POPC (1:1) with L/P = 5:1.

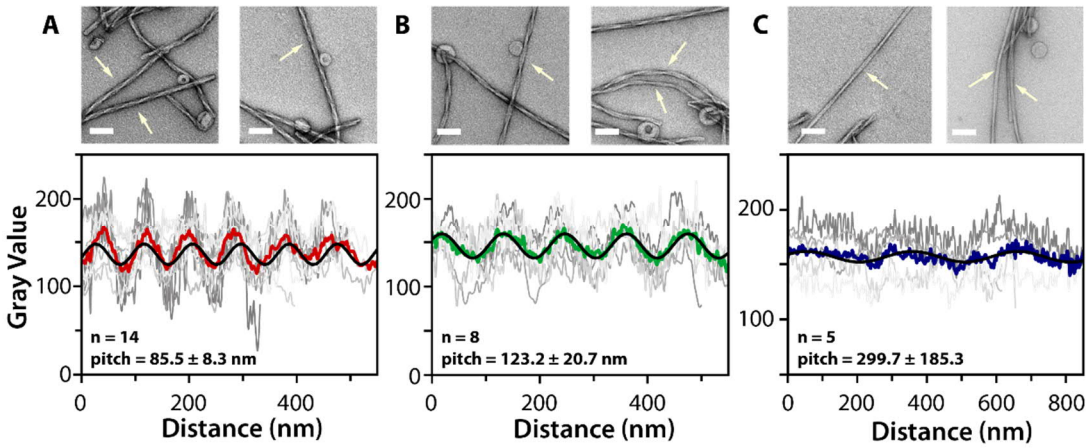

Fig. S4. Morphological analysis of αS fibrils in the presence of phospholipids. Top: TEM images of (A) high, (B) medium and (C) low pitch fibrils. Arrows indicate the corresponding fibril morphology. Bottom: Profile plots of the respective fibril morphology; gray plots represent raw, colored plots represent averaged data; black line represents sinusoidal fit to the averaged plot. Experiments were carried out with SUVs consisting of POPA and POPC (1:1) at a L/P ratio of 5:1.

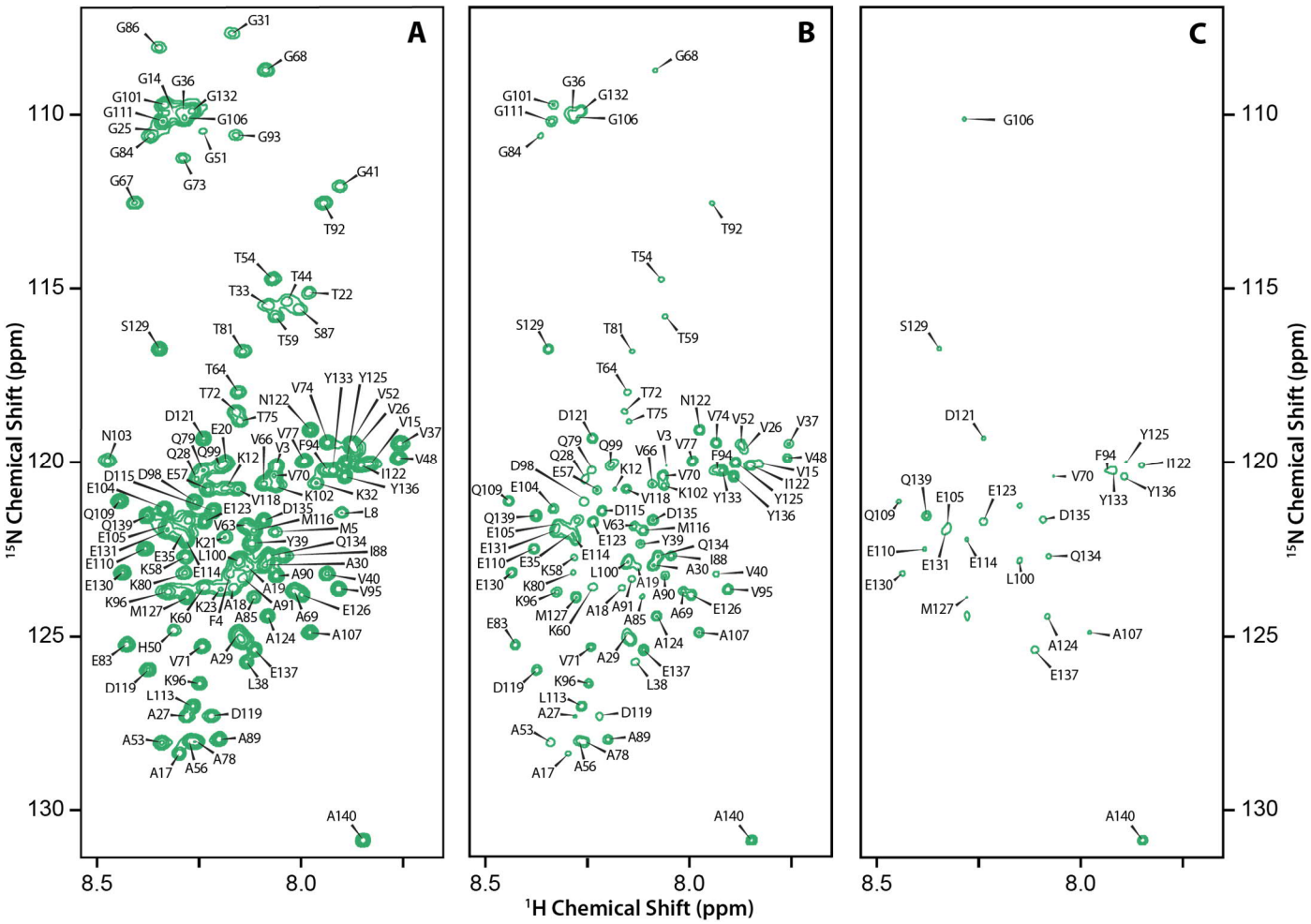

Fig. S5. Depletion of free monomeric **α**S during aggregation. ^{1}H-^{15}N-HSQC spectra of ^{15}N-labelled αS in the presence of vesicles of POPA and POPC (1:1, L/P = 10:1) acquired at (A) $t/t_{lag} = 0$ and after (B) $t/t_{lag} = 3.0$ and (C) $t/t_{lag} = 10.0$ showing the signal decrease of monomeric αS due to incorporation into large slowly tumbling aggregates.

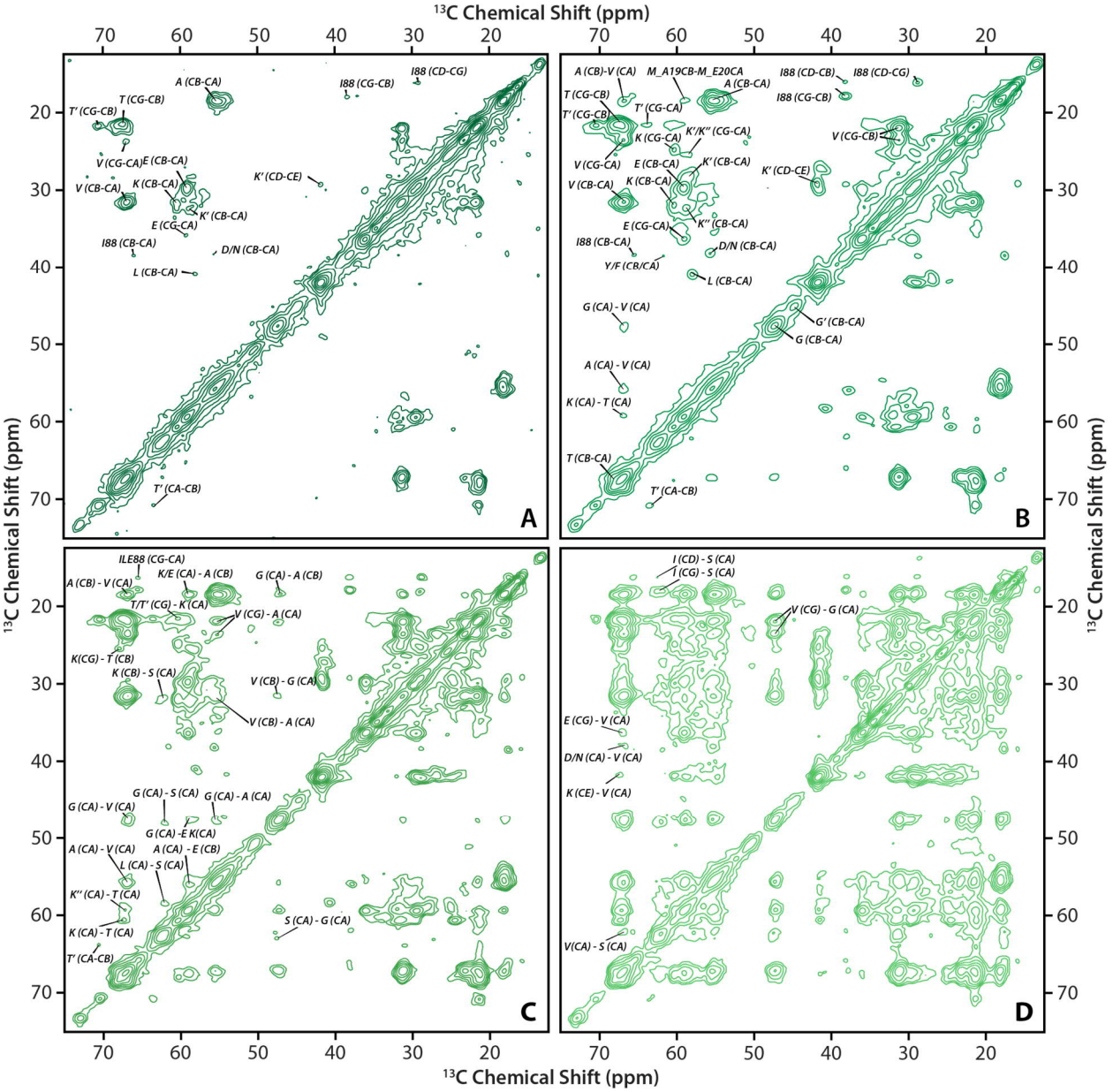

Fig. S6. Characterization of monomeric αS in the presence of phospholipids by ssNMR. 2D ^{13}C,^{13}C correlation spectra of U-^{13}C,^{15}N-αS monomers in the presence of POPA and POPC (1:1, L/P = 50:1) with DARR mixing of (A) 5 ms, (B) 20 ms, (C) 50 ms, (D) 200 ms. Spectra were acquired at 850 MHz with 17 kHz MAS at RT.

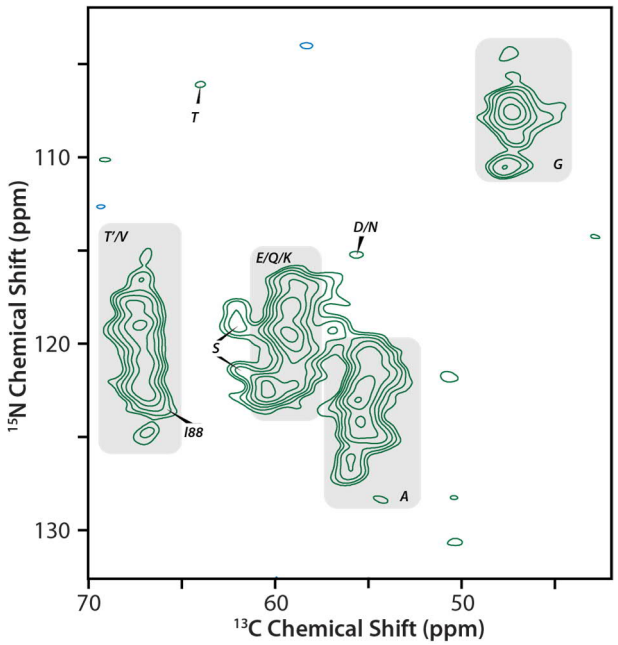

Figure S7. Backbone resonances of monomeric **α**S. 2D hNCA spectrum of U-^{13}C,^{15}N-αS monomers in the presence of POPA and POPC (1:1, L/P = 50:1) acquired at 850 MHz with 17 kHz spinning at RT. Sequential assignment was not possible, however distinct chemical shifts allow residue specific assignment. Gray boxes indicate residue types of the included peaks. Several ^{15}N-shifts with similar correlated ^{13}C-shifts are observed indicating the presence of multiple repeats of membrane bound helical αS.

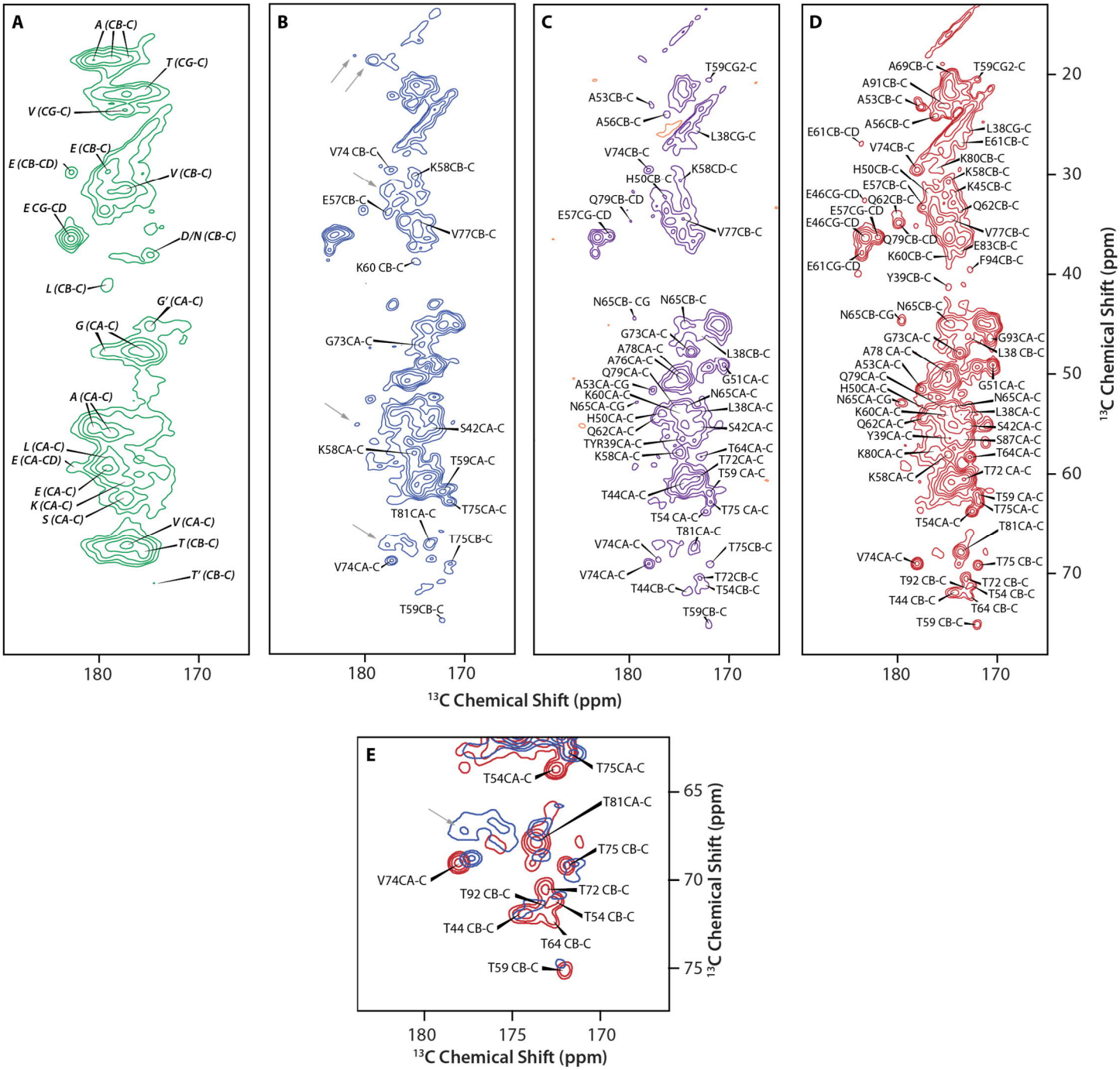

Fig. S8. Development of αS during aggregation. Carbonyl-region of 2D ^{13}C,^{13}C spectra of αS monomers (A), intermediate 1 (B), intermediate 2 (C) and fibrils (D) prepared in the presence of phospholipids. (E) Overlay of Threonine fingerprint region of Intermediate 1 (blue) on fibril spectra (red). Gray arrows indicate peaks indicative of a helical domain. All spectra were recorded with DARR-mixing of 20 ms at 850 MHz with 17 kHz MAS.

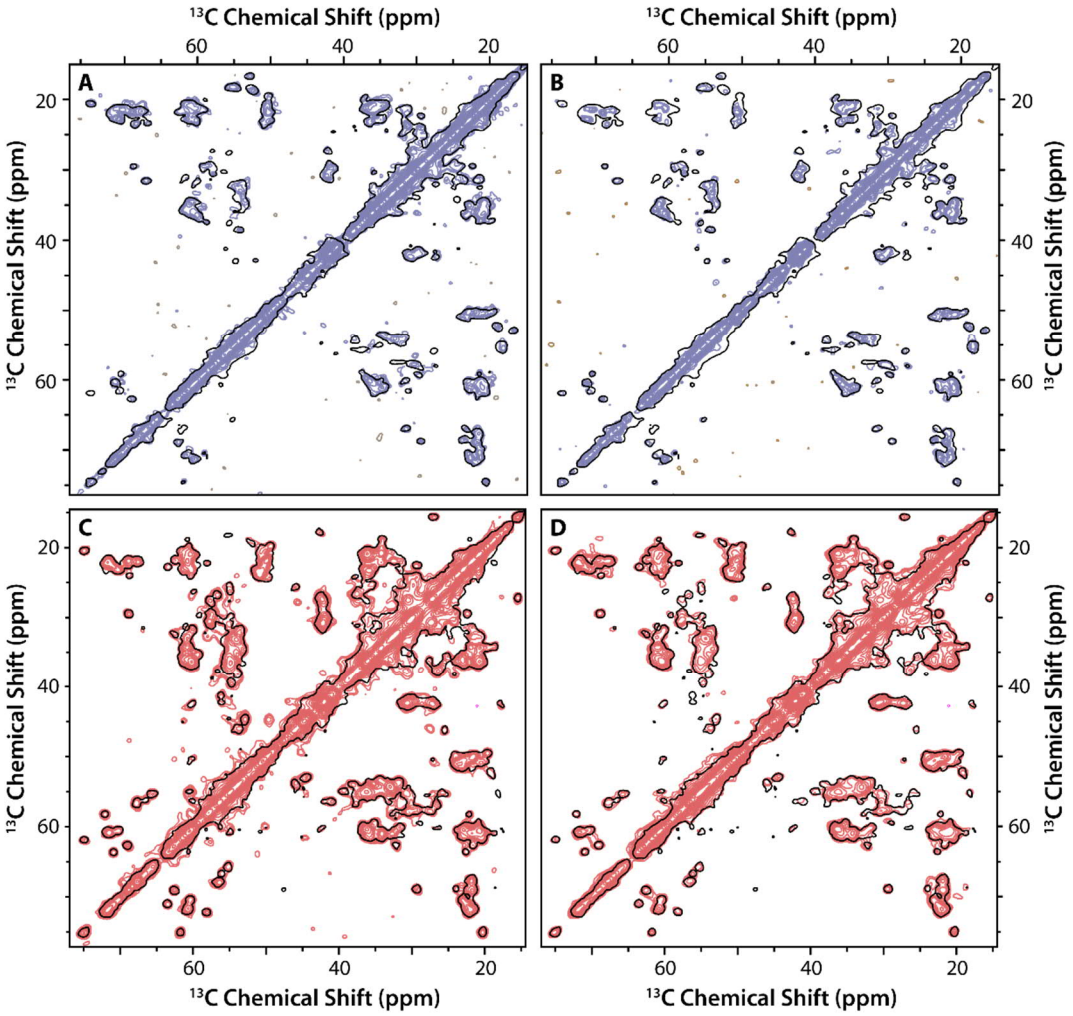

Fig. S9. Reproducibility of intermediates and fibrils. 2D ^{13}C,^{13}C spectra with DARR mixing (20 ms) of two replicates of αS intermediate 1 formed in the presence of POPA and POPC (1:1) at a L/P ratio of 10:1 (A & B) and αS fibrils formed at a L/P ratio of 10:1 (C) and 5:1(D) each recorded at 850 MHz with 17 kHz MAS compared to the spectra discussed in Fig. 5 and Fig. S8 (black outlines). Samples were prepared in under identical conditions. Spectra show similar sets of peaks, confirming reproducibility.

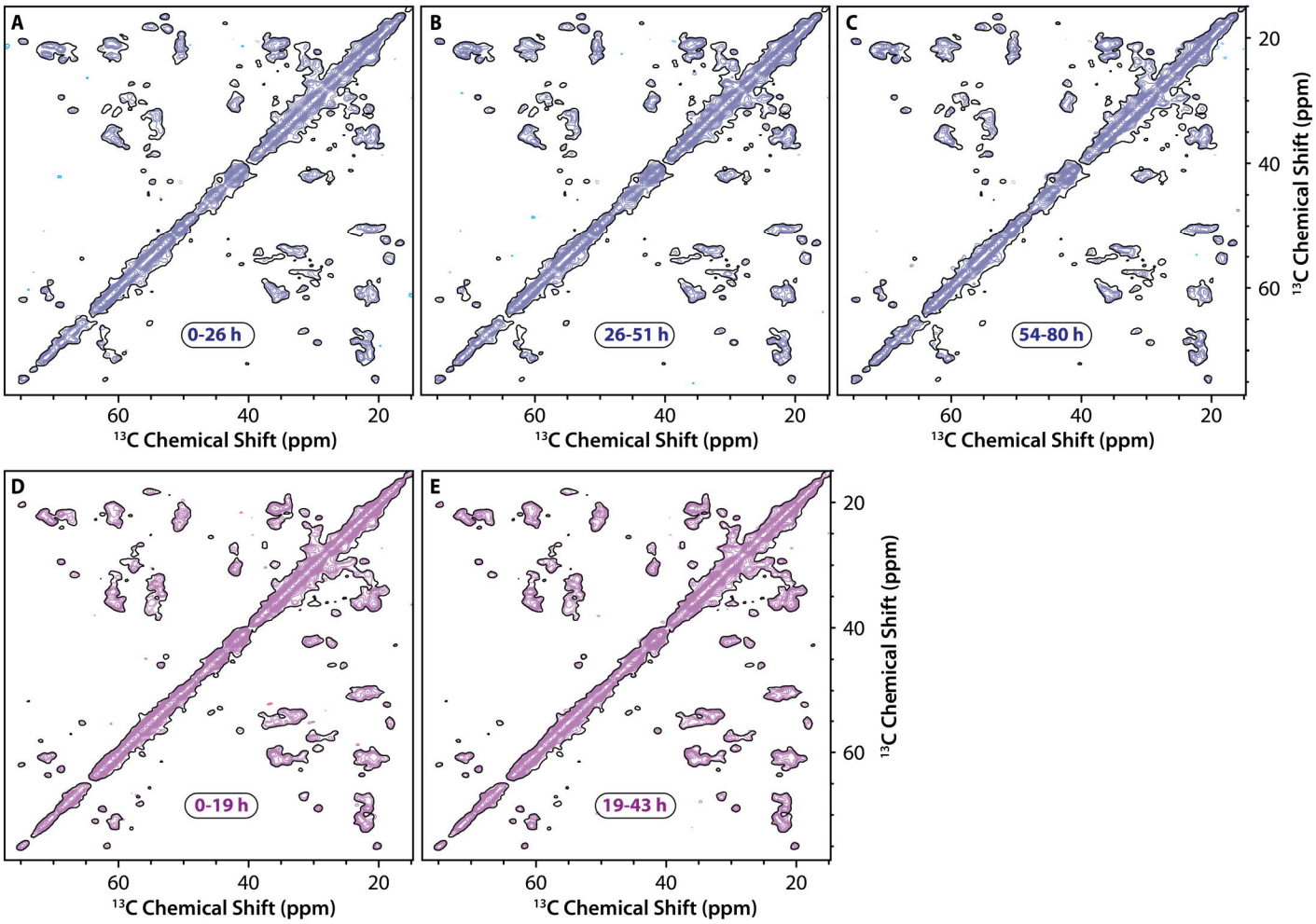

Fig. S10. Stability of intermediates 1 and 2. 2D ^{13}C,^{13}C spectra with DARR mixing (20 ms) of αS intermediate 1 and intermediate 2 recorded at 850 MHz with 17 kHz MAS at RT. Spectra show a sample of intermediate 1 from (A) 0-26 h, (B) 26-51 h and (C) 54-80 h and a sample of intermediate 2 from (D) 0-19 h and (E) 19-43 h, where 0 h is the beginning of measurement. Spectra added up from short blocks and show consistent sets of signals. Black outlines belong to spectra consisting of the sum of all blocks discussed in Fig. 5 and Fig. S8.

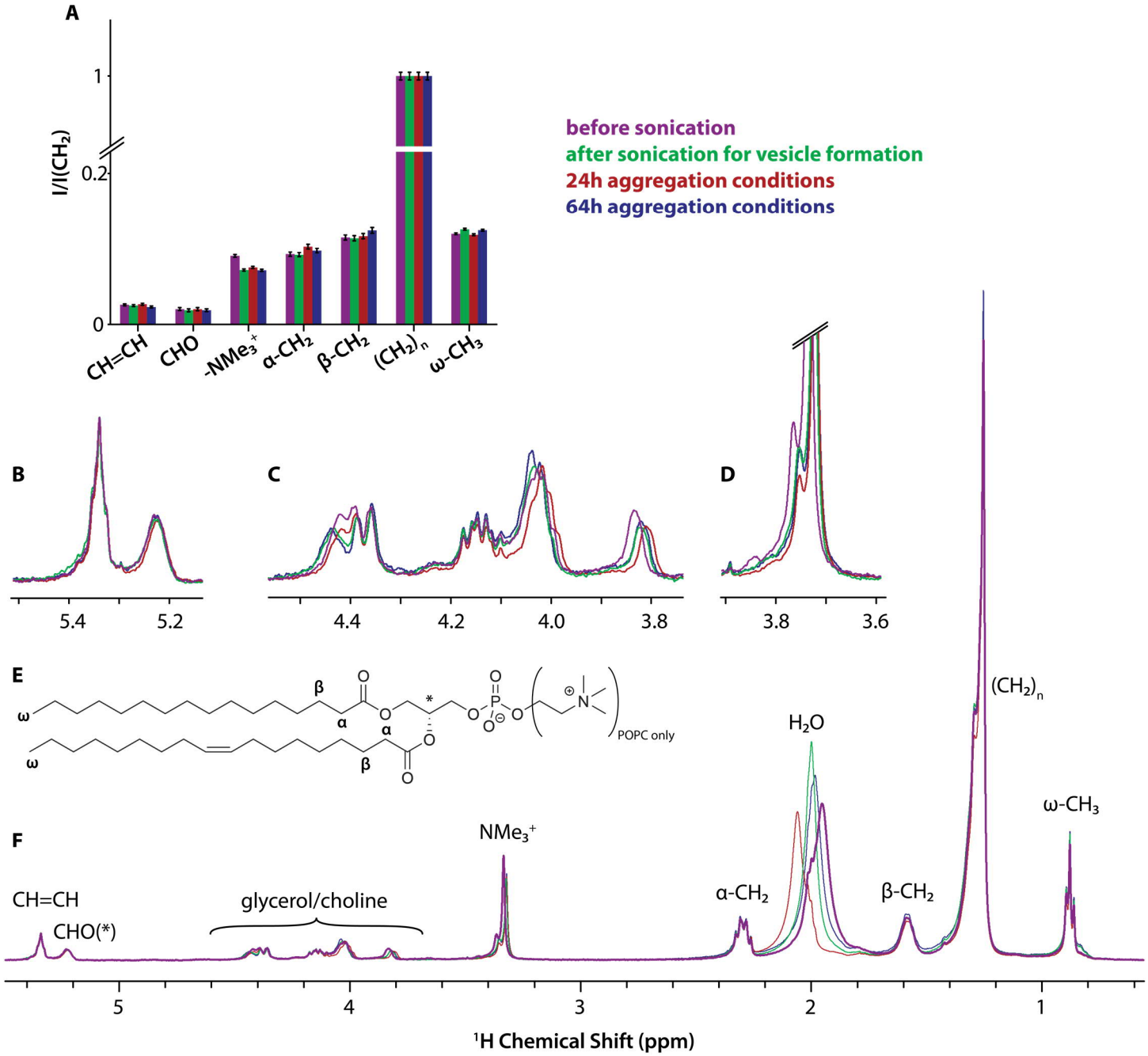

Fig. S11. Confirmation of lipid stability by NMR. POPA and POPC (1:1) were extracted from an aqueous solution before (purple) and after (green) sonication for SUV formation as well as after 24 h (red) and 64 h (blue) under aggregation conditions. (A) Comparison of intensities originating from lipid proton peaks in a ^{1}H NMR spectrum normalized by the acyl-chain CH_2 peak indicates unaltered lipid structure. (B-D) Magnified peaks from the ^{1}H NMR spectra corresponding to lipid glycerol, double bond and choline moieties. Head group protons show minor chemical shift differences originating from binding of lipid molecules to residual water. (E) Chemical structure of POPC and POPA (without choline group). (F) The full ^{1}H NMR spectra of lipids in $CDCl_3$. Data were recorded at 400 MHz at 298 K.

Supplementary Tables

i → i±1										i → i±2					i → i±n (n>2)				
ω_1			ω_2		d(Å)	ω_1			ω_2		d(Å)	ω_1			ω_2		d(Å)	ω_1			ω_2		d(Å)
L38	CB	-	Y39	CA	4.75	T72	CA	-	G73	CA	3.78	T44	CA	-	S42	CB	6.29	Y39	CB	-	Q79	CD	10.74
Y39	CB	-	L38	CA	4.86	T72	CB	-	G73	CA	4.90	E46	CB	-	T44	CB	7.55	V40	CB	-	T75	CA	6.91
T44	CB	-	K45	CA	4.42	G73	CA	-	T72	CA	3.78	V48	CB	-	E46	CD	6.70	S42	CA	-	T75	CB	5.72
H50	CB	-	G51	CA	4.64			-	T72	CB	4.90	V49	CA	-	G47	CA	6.40	T54	CA	-	T64	CA	8.68
G51	CA	-	H50	CA	3.78			-	V74	CA	3.69	T59	CB	-	E57	CA	5.87	A56	CB	-	T59	CB	4.45
V52	CB	-	G51	CA	4.82	V74	CA	-	G73	CA	3.69	V63	CA	-	N65	CG	5.82	Q62	CB	-	T54	CB	5.64
T54	CA	-	A53	CA	3.79	V74	CB	-	G73	CA	4.84	V63	CB	-	N65	CG	5.31	Q62	CG	-	T54	CB	5.08
		-	V55	CA	3.80			-	T75	CA	3.79	V63	CG	-	N65	CG	4.12	T64	CA	-	T54	CA	8.68
		-	V55	CB	4.79	T75	CA	-	A76	CA	3.81	T64	CB	-	Q62	CA	6.88	G67	CA	-	I88	CG1	4.27
T54	CB	-	A53	C	3.49	A76	CA	-	T75	CA	3.81	G68	CA	-	V66	CA	5.33			-	I88	CG2	6.34
		-	A53	CA	4.79			-	T75	CB	4.87	V70	CA	-	G68	CA	6.94			-	I88	CD1	3.98
A56	CA	-	E57	CA	3.78	Q79	CB	-	K80	CA	4.71	V70	CB	-	G68	CA	7.40	A69	CA	-	T81	CA	7.04
E57	CA	-	K58	CA	3.83	K80	CA	-	T81	CA	3.77	V71	CB	-	G69	CA	6.21	T72	CB	-	G51	CA	4.73
K58	CA	-	T59	CB	4.76	K80	CB	-	Q79	CD	4.72	T72	CA	-	V74	CA	6.80			-	A76	CA	7.10
K58	CB	-	E57	CD	7.24			-	T81	CA	4.85	V74	CA	-	A76	CA	5.99	T75	CA	-	S42	CB	5.25
T59	CA	-	K58	CA	3.79	T81	CA	-	K80	CA	3.77	V77	CB	-	T75	CB	6.64	T75	CB	-	V40	CA	7.15
T59	CB	-	K58	CA	4.76	V82	CB	-	T81	CA	4.81	Q79	CB	-	T81	CA	6.52	A76	CA	-	T72	CB	7.10
		-	K58	CB	6.07	S87	CA	-	I88	CA	3.81	K80	CA	-	V82	CA	6.50	A78	CA	-	T81	CA	5.86
		-	K60	C	4.46			-	I88	CB	4.71	T92	CA	-	F94	CA	6.23	T81	CA	-	A69	CA	7.04
K60	CA	-	T59	CA	3.78	I88	CA	-	S87	CA	3.81			-	F94	CB	5.96	I88	CG1	-	G67	CA	4.27
		-	T59	CB	4.16	I88	CG2	-	S87	CA	6.10	V95	CB	-	G93	CA	6.39		CD1	-	G67	CA	3.98
V63	CA	-	T64	CA	3.80	I88	CD1	-	S87	CA	5.88							A90	CA	-	N65	CB	6.66
	CB	-	T64	CB	5.78	T92	CA	-	G93	CA	3.78							T92	CB	-	V63	CB	5.49
N65	CB	-	T64	CA	4.77	G93	CA	-	T92	CB	4.54												

Table S1. Contacts of residues within αS fibrils. List of long-range contacts obtained from ^{13}C,^{13}C correlation spectrum with DARR mixing of 200 ms of U-^{13}C,^{15}N-αS fibrils; Columns show contacts of residues with their neighboring residues (i±1) or with residues separated by one (i±2) or more residues (i±n (n>2). The approximate distance cutoff for observed contacts is about 7 Å.(65) Contacts in conflict with PDB 6ssx (expected distance >7 Å) are highlighted in red.

Table S2. Experimental details of NMR experiments on αS in this work. *Accumulated experiment time obtained from adding the free induction decay (FID) of several experiments acquired for samples in ssNMR.

Exp.	NS	Field (T)	F3	F2	F1	$t3_{max}$ (ms)	$t2_{max}$ (ms)	$t1_{max}$ (ms)	t_{mix} (ms)	T (K)	MAS (kHz)	Expt. time (h)	Acc. Exp. * Time (h)	Sample
^{1}H NMR	64	16.4	-	-	16384 (^{1}H)	-	-	97	-	288	-	0.05	0.05	^{15}N-αS, POPC/POPA
^{1}H-^{15}N-HSQC	16	"	-	2048 (^{1}H)	256 (^{15}N)	-	122	67	-	"	-	1.60	1.60	"
(H)CANH	4	"	1024 (^{1}H)	168 (^{13}C)	96 (^{15}N)	18.8	10.7	14	-	293	55	39.67	39.67	^{2}H,^{13}C,^{15}N-αS-fib.;
(H)CONH	4	"	1024 (^{1}H)	120 (^{13}C)	64 (^{15}N)	21.3	5.0	1.2	-	"	"	16.35	32.70	"
(HCO)CA(CO)NH	4	"	1024 (^{1}H)	168 (^{13}C)	96 (^{15}N)	18.8	10.7	14	-	"	"	36.53	73.07	"
(H)CO(CA)NH	4	"	1024 (^{1}H)	120 (^{13}C)	64 (^{15}N)	21.3	5.0	1.2	-	"	"	16.85	67.40	"
(HCA)CB(CA)NH	4	"	1024 (^{1}H)	240 (^{13}C)	64 (^{15}N)	21.3	7.5	12	-	"	"	33.87	169.33	"
(HCA)CB(CACO)NH	4	"	1024 (^{1}H)	240 (^{13}C)	64 (^{15}N)	21.3	7.5	12	-	"	"	34.07	170.33	"
H(H)NH	8	"	1024 (^{1}H)	88 (^{15}N)	80 (^{15}N)	21.3	5.2	13.7	25	"	"	42.45	127.35	"
(H)CANH	4	22.3	4096 (^{1}H)	92 (^{13}C)	102 (^{15}N)	41	5.5	15.1		293	100	18.88	56.65	^{13}C,^{15}N-αS-fibril; POPC/POPA
(H)CONH	4	"	2048 (^{1}H)	134 (^{13}C)	94 (^{15}N)	36.1	14	14		"	"	24.02	48.03	"
(HCO)CA(CO)NH	4	"	2048 (^{1}H)	92 (^{13}C)	102 (^{15}N)	36.1	5.5	15.1		"	"	20.73	62.20	"
^{13}C^{13}C-DARR	8	20	-	1016 (^{13}C)	800 (^{15}N)	-	8.5	8.1	20	293	17	6.35	12.65	^{13}C,^{15}N-αS-fibril; POPC/POPA
"	8	"	-	"	"	-	"	"	200	"	"	7.17	14.33	"
"	8	"	-	"	"	-	"	"	20	"	"	3.18	79.78	Intermediate 1
"	8	"	-	"	"	-	"	"	20	"	"	3.19	41.67	Intermediate 2
"	8	"	-	"	"	-	8.6	8.1	5	"	"	6.10	6.10	Monomer
"	8	"	-	"	"	-	"	"	20	"	"	6.17	6.17	"
"	8	"	-	"	"	-	"	"	50	"	"	6.27	12.53	"
(H)NCA	16	"	-	4096 (^{13}C)	512(^{13}C)	-	43	37	-	"	"	4.10	8.20	"

Table S3. CP parameters and relaxation delays of ssNMR experiments in this work.

Exp.	^{1}H-^{13}C-CP					^{13}C-^{15}N-CP					^{15}N-^{1}H-CP					^{1}H-^{15}N-CP					Relax. Delay (s)
	t_{CP} (ms)	^{1}H-rf (kHz)	shape	^{13}C-rf (kHz)	Shape	t_{CP} (ms)	^{13}C-rf (kHz)	shape	^{15}N-rf (kHz)	shape	t_{CP} (ms)	^{15}N-rf (kHz)	shape	^{1}H-rf (kHz)	shape	t_{CP} (ms)	^{1}H-rf (kHz)	shape	^{15}N-rf (kHz)	shape	
(H)CANH	7.0	89	rectangle	39	80-100%	18.0	37	tangent	25	square	0.6	38	100-80%	87	100-80%	-	-	-	-	-	2.0
(H)CONH	7.0	101	rectangle	39	80-100%	18.0	37	tangent	25	square	0.5	38	100-80%	91	100-80%	-	-	-	-	-	1.7
(HCO)CA(CO)NH	7.0	89	rectangle	39	80-100%	18.0	37	tangent	25	square	0.6	38	100-80%	87	100-80%	-	-	-	-	-	2.0
(H)CO(CA)NH	7.0	101	rectangle	39	80-100%	18.0	37	tangent	25	square	0.5	38	100-80%	91	100-80%	-	-	-	-	-	1.7
(HCA)CB(CA)NH	4.0	100	rectangle	44	80-100%	18.0	37	tangent	25	square	0.5	38	100-80%	91	100-80%	-	-	-	-	-	1.7
(HCA)CB(CACO)NH	5.0	100	rectangle	44	80-100%	18.0	37	tangent	25	square	0.5	38	100-80%	91	100-80%	-	-	-	-	-	1.7
H(H)NH	-	-	-	-	-	-	-	-	-	-	0.6	38	100-80%	91	100-80%	1.0	95	80-100%	54	80-100%	2.5
(H)CANH	1.2	143	square	30	100-80%	11.0	42	100-80%	65	square	0.3	31	80-100%	139	80-100%	-	-	-	-	-	1.6
(H)CONH	2.9	124	square	23	100-80%	10.2	42	100-80%	65	square	0.4	31	80-100%	139	80-100%	-	-	-	-	-	1.6
(HCO)CA(CO)NH	1.2	124	square	23	100-80%	11.0	42	100-80%	65	square	0.4	31	80-100%	139	80-100%	-	-	-	-	-	1.8
$^{13}C^{13}C$-DARR	0.5	72	80-100%	61	80-100%	-	-	-	-	-	-	-	-	-	-	-	-	-	-	-	1.8
"	0.5	72	80-100%	61	80-100%	-	-	-	-	-	-	-	-	-	-	-	-	-	-	-	1.8
"	0.5	72	80-100%	61	80-100%	-	-	-	-	-	-	-	-	-	-	-	-	-	-	-	1.8
"	2.0	84	80-100%	61	80-100%	-	-	-	-	-	-	-	-	-	-	-	-	-	-	-	1.8
"	1.5	90	80-100%	61	80-100%	-	-	-	-	-	-	-	-	-	-	-	-	-	-	-	1.8
"	"	"	"	"	"	-	-	-	-	-	-	-	-	-	-	-	-	-	-	-	1.8
"	"	"	"	"	"	-	-	-	-	-	-	-	-	-	-	-	-	-	-	-	1.8
(H)NCA	-	-	-	-	-	1.6	20	100-90%	14	rectangle	-	-	-	-	-	0.5	69	80-100%	94	square	1.7

REFERENCES AND NOTES

1. R. Jakes, M. G. Spillantini, M. Goedert, Identification of two distinct synucleins from human brain. *FEBS Lett.* **345**, 27–32 (1994).
2. M. G. Spillantini, M. L. Schmidt, V. M. Y. Lee, J. Q. Trojanowski, R. Jakes, M. Goedert, α-synuclein in Lewy bodies. *Nature* **388**, 839–840 (1997).
3. W. R. G. Gibb, M. M. Esiri, A. J. Lees, Clinical and pathological features of diffuse cortical Lewy body disease (Lewy body dementia). *Brain* **110**, 1131–1153 (1987).
4. E. Gómez-Tortosa, K. Newell, M. C. Irizarry, J. L. Sanders, B. T. Hyman, α-Synuclein immunoreactivity in dementia with Lewy bodies: Morphological staging and comparison with ubiquitin immunostaining. *Acta Neuropathol.* **99**, 352–357 (2000).
5. A. Fanciulli, G. K. Wenning, Multiple-system atrophy. *New Engl. J. Med.* **372**, 249–263 (2015).
6. J. G. Graham, D. R. Oppenheimer, Orthostatic hypotension and nicotine sensitivity in a case of multiple system atrophy. *J. Neurol. Neurosurg. Psychiatry* **32**, 28–34 (1969).
7. M. D. Tuttle, G. Comellas, A. J. Nieuwkoop, D. J. Covell, D. A. Berthold, K. D. Kloepper, J. M. Courtney, J. K. Kim, A. M. Barclay, A. Kendall, W. Wan, G. Stubbs, C. D. Schwieters, V. M. Y. Lee, J. M. George, C. M. Rienstra, Solid-state NMR structure of a pathogenic fibril of full-length human α-synuclein. *Nat. Struct. Mol. Biol.* **23**, 409–415 (2016).
8. B. Li, P. Ge, K. A. Murray, P. Sheth, M. Zhang, G. Nair, M. R. Sawaya, W. S. Shin, D. R. Boyer, S. Ye, D. S. Eisenberg, Z. H. Zhou, L. Jiang, Cryo-EM of full-length α-synuclein reveals fibril polymorphs with a common structural kernel. *Nat. Commun.* **9**, 3609 (2018).
9. R. Guerrero-Ferreira, N. M. I. Taylor, A.-A. Arteni, P. Kumari, D. Mona, P. Ringler, M. Britschgi, M. E. Lauer, A. Makky, J. Verasdonck, R. Riek, R. Melki, B. H. Meier, A. Böckmann, L. Bousset, H. Stahlberg, Two new polymorphic structures of human full-length alpha-synuclein fibrils solved by cryo-electron microscopy. *eLife* **8**, e48907 (2019).
10. P. C. Ke, M.-A. Sani, F. Ding, A. Kakinen, I. Javed, F. Separovic, T. P. Davis, R. Mezzenga, Implications of peptide assemblies in amyloid diseases. *Chem. Soc. Rev.* **46**, 6492–6531 (2017).
11. B. I. Giasson, I. V. J. Murray, J. Q. Trojanowski, V. M. Y. Lee, A hydrophobic stretch of 12 amino acid residues in the middle of α-synuclein is essential for filament assembly. *J. Biol. Chem.* **276**, 2380–2386 (2001).
12. S. W. Chen, S. Drakulic, E. Deas, M. Ouberai, F. A. Aprile, R. Arranz, S. Ness, C. Roodveldt, T. Guilliams, E. J. De-Genst, D. Klenerman, N. W. Wood, T. P. J. Knowles, C. Alfonso, G. Rivas, A.

Y. Abramov, J. M. Valpuesta, C. M. Dobson, N. Cremades, Structural characterization of toxic oligomers that are kinetically trapped during α-synuclein fibril formation. *Proc. Natl. Acad. Sci. U.S.A.* **112**, E1994–E2003 (2015).

13. N. Plotegher, E. Greggio, M. Bisaglia, L. Bubacco, Biophysical groundwork as a hinge to unravel the biology of α-synuclein aggregation and toxicity. *Q. Rev. Biophys.* **47**, 1–48 (2014).
14. H. Roberts, D. Brown, Seeking a mechanism for the toxicity of oligomeric α-synuclein. *Biomolecules* **5**, 282–305 (2015).
15. G. Fusco, S. W. Chen, P. T. F. Williamson, R. Cascella, M. Perni, J. A. Jarvis, C. Cecchi, M. Vendruscolo, F. Chiti, N. Cremades, L. Ying, C. M. Dobson, A. De Simone, Structural basis of membrane disruption and cellular toxicity by α-synuclein oligomers. *Science* **358**, 1440–1443 (2017).
16. H. A. Lashuel, B. M. Petre, J. Wall, M. Simon, R. J. Nowak, T. Walz, P. T. Lansbury Jr., α-Synuclein, especially the Parkinson's disease-associated mutants, forms pore-like annular and tubular protofibrils. *J. Mol. Biol.* **322**, 1089–1102 (2002).
17. D. Sulzer, R. H. Edwards, The physiological role of α-synuclein and its relationship to Parkinson's disease. *J. Neurochem.* **150**, 475–486 (2019).
18. R. J. Perrin, W. S. Woods, D. F. Clayton, J. M. George, Interaction of human α-synuclein and Parkinson's disease variants with phospholipids. Structural analysis using site-directed mutagenesis. *J. Biol. Chem.* **275**, 34393–34398 (2000).
19. D. Eliezer, E. Kutluay, R. Bussell, G. Browne, Conformational properties of α-synuclein in its free and lipid-associated states. *J. Mol. Biol.* **307**, 1061–1073 (2001).
20. C. Galvagnion, A. K. Buell, G. Meisl, T. C. T. Michaels, M. Vendruscolo, T. P. J. Knowles, C. M. Dobson, Lipid vesicles trigger α-synuclein aggregation by stimulating primary nucleation. *Nat. Chem. Biol.* **11**, 229–234 (2015).
21. C. Galvagnion, J. W. P. Brown, M. M. Ouberai, P. Flagmeier, M. Vendruscolo, A. K. Buell, E. Sparr, C. M. Dobson, Chemical properties of lipids strongly affect the kinetics of the membrane-induced aggregation of α-synuclein. *Proc. Natl. Acad. Sci. U.S.A.* **113**, 7065–7070 (2016).
22. G. Comellas, L. R. Lemkau, D. H. Zhou, J. M. George, C. M. Rienstra, Structural intermediates during α-synuclein fibrillogenesis on phospholipid vesicles. *J. Am. Chem. Soc.* **134**, 5090–5099 (2012).

23. D. H. Zhou, G. Shah, M. Cormos, C. Mullen, D. Sandoz, C. M. Rienstra, Proton-detected solid-state NMR spectroscopy of fully protonated proteins at 40 kHz magic-angle spinning. *J. Am. Chem. Soc.* **129**, 11791–11801 (2007).
24. Y. Shen, F. Delaglio, G. Cornilescu, A. Bax, TALOS+: A hybrid method for predicting protein backbone torsion angles from NMR chemical shifts. *J. Biomol. NMR* **44**, 213–223 (2009).
25. J. Gath, L. Bousset, B. Habenstein, R. Melki, B. H. Meier, A. Böckmann, Yet another polymorph of α-synuclein: Solid-state sequential assignments. *Biomol. NMR Assign.* **8**, 395–404 (2014).
26. D. R. Boyer, B. Li, C. Sun, W. Fan, K. Zhou, M. P. Hughes, M. R. Sawaya, L. Jiang, D. S. Eisenberg, The α-synuclein hereditary mutation E46K unlocks a more stable, pathogenic fibril structure. *Proc. Natl. Acad. Sci. U.S.A.* **117**, 3592–3602 (2020).
27. C. Seuring, J. Verasdonck, P. Ringler, R. Cadalbert, H. Stahlberg, A. Böckmann, B. H. Meier, R. Riek, Amyloid fibril polymorphism: Almost identical on the atomic level, mesoscopically very different, *J. Phys. Chem. B* **121**, 1783–1792 (2017).
28. A. Chaari, H. Horchani, F. Frikha, R. Verger, Y. Gargouri, M. Ladjimi, Surface behavior of α-synuclein and its interaction with phospholipids using the Langmuir monolayer technique: A comparison between monomeric and fibrillar α-synuclein. *Int. J. Biol. Macromol.* **58**, 190–198 (2013).
29. A. Iyer, M. M. A. E. Claessens, Disruptive membrane interactions of alpha-synuclein aggregates. *Biochim. Biophys. Acta Proteins Proteomics* **1867**, 468–482 (2019).
30. E. E. Najbauer, K. T. Movellan, T. Schubeis, T. Schwarzer, K. Castiglione, K. Giller, G. Pintacuda, S. Becker, L. B. Andreas, Probing membrane protein insertion into lipid bilayers by solid-state NMR. *ChemPhysChem* **20**, 302–310 (2019).
31. E. K. Paulson, C. R. Morcombe, V. Gaponenko, B. Dancheck, R. A. Byrd, K. W. Zilm, High-sensitivity observation of dipolar exchange and NOEs between exchangeable protons in proteins by 3D solid-state NMR spectroscopy. *J. Am. Chem. Soc.* **125**, 14222–14223 (2003).
32. H. Flyvbjerg, E. Jobs, S. Leibler, Kinetics of self-assembling microtubules: An “inverse problem” in biochemistry. *Proc. Natl. Acad. Sci. U.S.A.* **93**, 5975–5979 (1996).
33. C. R. Bodner, C. M. Dobson, A. Bax, Multiple tight phospholipid-binding modes of α-synuclein revealed by solution NMR spectroscopy. *J. Mol. Biol.* **390**, 775–790 (2009).

34. A. Quist, I. Doudevski, H. Lin, R. Azimova, D. Ng, B. Frangione, B. Kagan, J. Ghiso, R. Lal, Amyloid ion channels: A common structural link for protein-misfolding disease. *Proc. Natl. Acad. Sci. U.S.A.* **102**, 10427–10432 (2005).
35. G. Meisl, J. B. Kirkegaard, P. Arosio, T. C. T. Michaels, M. Vendruscolo, C. M. Dobson, S. Linse, T. P. J. Knowles, Molecular mechanisms of protein aggregation from global fitting of kinetic models. *Nat. Protoc.* **11**, 252–272 (2016).
36. D. S. Wishart, B. D. Sykes, The 13C chemical-shift index: A simple method for the identification of protein secondary structure using 13C chemical-shift data. *J. Biomol. NMR* **4**, 171–180 (1994).
37. G. Fusco, A. De Simone, T. Gopinath, V. Vostrikov, M. Vendruscolo, C. M. Dobson, G. Veglia, Direct observation of the three regions in α-synuclein that determine its membrane-bound behaviour. *Nat. Commun.* **5**, 3827 (2014).
38. M. Drescher, F. Godschalk, G. Veldhuis, B. D. van Rooijen, V. Subramaniam, M. Huber, Spin-label EPR on α-synuclein reveals differences in the membrane binding affinity of the two antiparallel helices. *Chembiochem* **9**, 2411–2416 (2008).
39. C. C. Jao, B. G. Hegde, J. Chen, I. S. Haworth, R. Langen, Structure of membrane-bound α-synuclein from site-directed spin labeling and computational refinement. *Proc. Natl. Acad. Sci. U.S.A.* **105**, 19666–19671 (2008).
40. S. M. Kashid, S. Bagchi, Experimental determination of the electrostatic nature of carbonyl hydrogen-bonding interactions using IR-NMR correlations. *J. Phys. Chem. Lett.* **5**, 3211–3215 (2014).
41. N. Lorenzen, S. B. Nielsen, A. K. Buell, J. D. Kaspersen, P. Arosio, B. S. Vad, W. Paslawski, G. Christiansen, Z. Valnickova-Hansen, M. Andreasen, J. J. Enghild, J. S. Pedersen, C. M. Dobson, T. P. J. Knowles, D. E. Otzen, The role of stable α-synuclein oligomers in the molecular events underlying amyloid formation. *J. Am. Chem. Soc.* **136**, 3859–3868 (2014).
42. K. Vamvaca, M. J. Volles, P. T. Lansbury, The first N-terminal amino acids of α-synuclein are essential for α-helical structure formation in vitro and membrane binding in yeast. *J. Mol. Biol.* **389**, 413–424 (2009).
43. R. W. Newberry, J. T. Leong, E. D. Chow, M. Kampmann, W. F. DeGrado, Deep mutational scanning reveals the structural basis for α-synuclein activity. *Nat. Chem. Biol.*, (2020), 16, 653, 659.

44. L. Fonseca-Ornelas, S. E. Eisbach, M. Paulat, K. Giller, C. O. Fernández, T. F. Outeiro, S. Becker, M. Zweckstetter, Small molecule-mediated stabilization of vesicle-associated helical α-synuclein inhibits pathogenic misfolding and aggregation. *Nat. Commun.* **5**, 5857 (2014).
45. G. Fusco, T. Pape, A. D. Stephens, P. Mahou, A. R. Costa, C. F. Kaminski, G. S. Kaminski Schierle, M. Vendruscolo, G. Veglia, C. M. Dobson, A. De Simone, Structural basis of synaptic vesicle assembly promoted by α-synuclein. *Nat. Commun.* **7**, 12563 (2016).
46. N. P. Reynolds, A. Soragni, M. Rabe, D. Verdes, E. Liverani, S. Handschin, R. Riek, S. Seeger, Mechanism of membrane interaction and disruption by α-synuclein. *J. Am. Chem. Soc.* **133**, 19366–19375 (2011).
47. S. H. Shahmoradian, A. J. Lewis, C. Genoud, J. Hench, T. E. Moors, P. P. Navarro, D. Castaño-Díez, G. Schweighauser, A. Graff-Meyer, K. N. Goldie, R. Sütterlin, E. Huisman, A. Ingrassia, Y. d. Gier, A. J. M. Rozemuller, J. Wang, A. D. Paepe, J. Erny, A. Staempfli, J. Hoernschemeyer, F. Großerüschkamp, D. Niedieker, S. F. El-Mashtoly, M. Quadri, W. F. J. Van Ijcken, V. Bonifati, K. Gerwert, B. Bohrmann, S. Frank, M. Britschgi, H. Stahlberg, W. D. J. Van de Berg, M. E. Lauer, Lewy pathology in Parkinson's disease consists of crowded organelles and lipid membranes. *Nat. Neurosci.* **22**, 1099–1109 (2019).
48. F. Peccati, S. Pantaleone, V. Riffet, X. Solans-Monfort, J. Contreras-García, V. Guallar, M. Sodupe, Binding of thioflavin T and related probes to polymorphic models of amyloid-β fibrils. *J. Phys. Chem. B* **121**, 8926–8934 (2017).
49. A. I. Sulatskaya, N. P. Rodina, M. I. Sulatsky, O. I. Povarova, I. A. Antifeeva, I. M. Kuznetsova, K. K. Turoverov, Investigation of α-synuclein amyloid fibrils using the fluorescent probe thioflavin T. *Int. J. Mol. Sci.* **19**, 2486 (2018).
50. M. S. Celej, R. Sarroukh, E. Goormaghtigh, G. D. Fidelio, J.-M. Ruysschaert, V. Raussens, Toxic prefibrillar α-synuclein amyloid oligomers adopt a distinctive antiparallel β-sheet structure. *Biochem. J.* **443**, 719–726 (2012).
51. C. P. A. Doherty, S. M. Ulamec, R. Maya-Martinez, S. C. Good, J. Makepeace, G. N. Khan, P. van Oosten-Hawle, S. E. Radford, D. J. Brockwell, A short motif in the N-terminal region of α-synuclein is critical for both aggregation and function. *Nat. Struct. Mol. Biol.* **27**, 249–259 (2020).
52. S. Esteban-Martín, J. Silvestre-Ryan, Carlos W. Bertoncini, X. Salvatella, Identification of fibril-like tertiary contacts in soluble monomeric α-synuclein. *Biophys. J.* **105**, 1192–1198 (2013).

53. N. Rezaei-Ghaleh, G. Parigi, A. Soranno, A. Holla, S. Becker, B. Schuler, C. Luchinat, M. Zweckstetter, Local and global dynamics in intrinsically disordered synuclein. *Angew. Chem. Int. Ed.* **57**, 15262–15266 (2018).
54. A. Sidhu, I. Segers-Nolten, V. Raussens, M. M. A. E. Claessens, V. Subramaniam, Distinct mechanisms determine α-synuclein fibril morphology during growth and maturation. *ACS Chem. Neurosci.* **8**, 538–547 (2017).
55. M. Schweighauser, Y. Shi, A. Tarutani, F. Kametani, A. G. Murzin, B. Ghetti, T. Matsubara, T. Tomita, T. Ando, K. Hasegawa, S. Murayama, M. Yoshida, M. Hasegawa, S. H. W. Scheres, M. Goedert, Structures of α-synuclein filaments from multiple system atrophy. *Nature* **585**, 464–469 (2020).
56. W. Hoyer, T. Antony, D. Cherny, G. Heim, T. M. Jovin, V. Subramaniam, Dependence of α-synuclein aggregate morphology on solution conditions. *J. Mol. Biol.* **322**, 383–393 (2002).
57. F. Delaglio, S. Grzesiek, G. W. Vuister, G. Zhu, J. Pfeifer, A. Bax, NMRPipe: A multidimensional spectral processing system based on UNIX pipes. *J. Biomol. NMR* **6**, 277–293 (1995).
58. W. F. Vranken, W. Boucher, T. J. Stevens, R. H. Fogh, A. Pajon, M. Llinas, E. L. Ulrich, J. L. Markley, J. Ionides, E. D. Laue, The CCPN data model for NMR spectroscopy: Development of a software pipeline. *Proteins* **59**, 687–696 (2005).
59. V. Shabardina, C. Kramer, B. Gerdes, J. Braunger, A. Cordes, J. Schäfer, I. Mey, D. Grill, V. Gerke, C. Steinem, Mode of ezrin-membrane interaction as a function of PIP2 binding and pseudophosphorylation. *Biophys. J.* **110**, 2710–2719 (2016).
60. J. Schindelin, I. Arganda-Carreras, E. Frise, V. Kaynig, M. Longair, T. Pietzsch, S. Preibisch, C. Rueden, S. Saalfeld, B. Schmid, J.-Y. Tinevez, D. J. White, V. Hartenstein, K. Eliceiri, P. Tomancak, A. Cardona, Fiji: An open-source platform for biological-image analysis. *Nat. Methods* **9**, 676–682 (2012).
61. A. Böckmann, C. Gardiennet, R. Verel, A. Hunkeler, A. Loquet, G. Pintacuda, L. Emsley, B. H. Meier, A. Lesage, Characterization of different water pools in solid-state NMR protein samples. *J. Biomol. NMR* **45**, 319–327 (2009).
62. E. Barbet-Massin, A. J. Pell, J. S. Retel, L. B. Andreas, K. Jaudzems, W. T. Franks, A. J. Nieuwkoop, M. Hiller, V. Higman, P. Guerry, A. Bertarello, M. J. Knight, M. Felletti, T. Le Marchand, S. Kotelovica, I. Akopjana, K. Tars, M. Stoppini, V. Bellotti, M. Bolognesi, S. Ricagno, J. J. Chou, R. G. Griffin, H. Oschkinat, A. Lesage, L. Emsley, T. Herrmann, G. Pintacuda, Rapid

proton-detected NMR assignment for proteins with fast magic angle spinning. *J. Am. Chem. Soc.* **136**, 12489–12497 (2014).

63. E. E. Najbauer, L. B. Andreas, Correcting for magnetic field drift in magic-angle spinning NMR datasets. *J. Magn. Reson.* **305**, 1–4 (2019).
64. W. Lee, M. Tonelli, J. L. Markley, NMRFAM-SPARKY: Enhanced software for biomolecular NMR spectroscopy. *Bioinformatics* **31**, 1325–1327 (2014).
65. M. Roos, V. S. Mandala, M. Hong, Determination of long-range distances by fast magic-angle-spinning radiofrequency-driven ^{19}F–^{19}F dipolar recoupling NMR. *J. Phys. Chem. B* **122**, 9302–9313 (2018).